J Mater Sci (2018) 53:1743–1757

Ceramics

Hydration kinetics and morphology of cement pastes with pozzolanic volcanic ash studied via synchrotron-based techniques

Kunal Kupwade-Patil[1,*], Stephanie Chin[1], Jan Ilavsky[2], Ross N. Andrews[2], Ali Bumajdad[3], and Oral Büyüköztürk[1,*]

[1] *Laboratory for Infrastructure Science and Sustainability (LISS), Department of Civil and Environmental Engineering, Massachusetts Institute of Technology, Cambridge, MA 02139, USA*

[2] *X-ray Science Division, Advanced Photon Source, Argonne National Laboratory, Lemont, IL 60439, USA*

[3] *Chemistry Department, Kuwait University, P.O. Box 5969, 13060 Safat, Kuwait*

Received: 14 August 2017
Accepted: 5 October 2017
Published online: 13 October 2017

ABSTRACT

This study investigates the early ages of hydration behavior when basaltic volcanic ash was used as a partial substitute to ordinary Portland cement using ultra-small-angle X-ray scattering and wide-angle X-ray scattering (WAXS). The mix design consisted of 10, 30 and 50% substitution of Portland cement with two different-sized volcanic ashes. The data showed that substitution of volcanic ash above 30% results in excess unreacted volcanic ash, rather than additional pozzolanic reactions along longer length scales. WAXS studies revealed that addition of finely ground volcanic ash facilitated calcium-silicate-hydrate related phases, whereas inclusion of coarser volcanic ash caused domination by calcium-aluminum-silicate-hydrate and unreacted MgO phases, suggesting some volcanic ash remained unreacted throughout the hydration process. Addition of more than 30% volcanic ash leads to coarser morphology along with decreased surface area and higher intensity of scattering at early-age hydration. This suggests an abrupt dissolution indicated by changes in surface area due to the retarding gel formation that can have implication on early-age setting influencing the mechanical properties of the resulting cementitious matrix. The findings from this work show that the concentration of volcanic ash influences the specific surface area and morphology of hydration products during the early age of hydration. Hence, natural pozzolanic volcanic ashes can be a viable substitute to Portland cement by providing environmental benefits in terms of lower-carbon footprint along with long-term durability.

Address correspondence to E-mail: kunalk@mit.edu; obuyuk@mit.edu

DOI 10.1007/s10853-017-1659-4

Introduction

Cement hydration is a complex process that involves the formation of colloidal structures in its aqueous phase [1]. This hydration process, with its colloidal-formed structure, usually occurs in the presence of additives, or supplementary cementitious materials (SCMs). The morphological nature of such formed structures in the presence of additives plays an important role in determining the setting, aging and mechanical properties of the resulting composite material. SCMs are mixed into the Portland cement prior to adding water; as soon as the water comes in contact with the mix, the SCMs react and form hydration products. Such hydrated inorganic products (sol) undergo a slow condensation reaction (gel) with continual increase in the silicate (the most abundant chemicals in cement paste) chain length and more cross-linking. Hence, as time passes, a dense matrix is formed. The range of colloidal microstructures can be determined/studied using scattering techniques. Since the gel is relatively condensed, synchrotron-/X-ray-based scattering technique will be useful to study the size of the prism-like/globules/fractals (irregular/fragmented shape) formed during the hydration process [2–7]. At an early age of the cement paste hydration reaction, the globule size and its aggregates are expected to be in the range of $\sim$ 1 nm–10 μm. This range of size can be studied by ultra-small-angle X-ray scattering (USAXS) (1 nm–10 μm). Additionally, small-angle scattering techniques are helpful for determining in situ the early-age surface area of the cement paste as a function of time. This is not possible with other techniques; for example, N_2 sorptiometry requires a relatively dry sample. To date, limited research has been performed using synchrotron techniques to study the early-age hydration product formation when SCMs are mixed with Portland cements [8–15]. An in-depth insight into the resulting microstructure will help in providing systematic guidelines for selection of the optimum content and type of additive for developing functionalized and engineered durable concretes.

Mixing SCM with Portland cement leads to hydration products of complex morphology. Small-angle neutron/X-ray scattering (SANS/SAXS) are powerful noninvasive techniques for examining complex microstructure of hydration products. In recent years, small-angle scattering has been used extensively to study the volume and surface fractal dimensions of C-S-H and the water inside the porous medium [7, 16–18]. Dynamic time evolution of hydrating ordinary Portland cement (OPC) microstructure at an early age has been studied by various researchers [2, 8, 15, 18–21]. Sequential time evolution starts with the dissolution of aluminosilicates, followed by nucleation and initial gel formation. Gelation is succeeded by reorganization and polymerization, leading to hardening of the cement paste. Recently, SANS was used to detect the lamellar structure and interface between water and hydrated C-S-H layers [18]. This SANS study had determined the globule morphology of C-S-H with alternating layers of water and calcium silicate layers. An analytical model was used to relate the water content inside the layers of C-S-H determining the changes in the morphology of C-S-H globules [18].

Allen et al. [6] characterized C-S-H using USAXS/SANS and obtained the structure of C-S-H as a globule, although recent studies show the C-S-H has disk-like structure [2, 18]. Additives to Portland cement diversify/increase the formation of hydration products, including calcium-aluminum-silicate-hydrate (C-A-S-H) and magnesium-silicate-hydrate (M-S-H). Recent work has shown that M-S-H has a spherical morphology with an average radius of 17 nm [22]. Portland cements mixed with additives result in a complex phase morphology, which is difficult to decipher as the structures are formed at various length scales.

Most small-angle scattering studies have been performed on pure C-S-H gel-based systems [6, 7, 18], but few have been performed on Portland cements mixed with SCM [2, 8]. Current studies show that volcanic ash from Saudi Arabia can be an excellent SCM for up to 30% substitution of Portland cement [23–25]. This volcanic ash is rich in aluminosilicate and possesses pozzolanic properties. It is produced by an active volcano in the Arabian Gulf region in Saudi Arabia, which also generates a significant amount of volcanic rocks. Significant energy and manpower have been used to send this volcanic rock as waste to landfills. Therefore, there is an abundance of volcanic ash or volcanic rocks pulverized to a powder that can be used as a SCM. Successful utilization of volcanic ash in Portland cements can provide an economic and environmentally friendly

solution to natural waste disposal in the Arabian Gulf and other regions.

The purpose of this study is to provide an insight into early-age hydration mechanism when Portland cement is partially replaced by pozzolanic volcanic ash. A critical insight into engineering mix design is provided using in situ experiments at various length scales, from nano- to micrometer. The combination of USAXS/SAXS/WAXS helps in determining the microstructure in terms of surface area and phases resulting due to the addition of volcanic ash. Complex morphology of cement paste has an extended range of structural length scales (from 1 nm to a few μm), which control various aspects of their in-service performance. It is therefore critical to simultaneously characterize as large range of sizes as possible with one technique, on the same volume of sample, and at the same time (as oppose to in separate experiments). Such measurement provides results with much less ambiguity related to sample homogeneity and sample/experimental conditions reproducibility.

The current work examines the effect of the concentration and particle size of volcanic ash when it is used as a partial replacement to Portland cement. Surface area per unit volume was extracted at specific time intervals using USAXS data to investigate the effect of volcanic ash concentration during early period of hydration. Additionally, phases were identified using WAXS analysis at intermittent time intervals to examine the progression of the first 2 months of hydration. The findings from this study provide a basis for understanding the morphology and growth of hydration products that could affect the rheological and mechanical properties of the resulting cementitious binder. To the best of our knowledge, this is the first time the influence of volcanic ash additives on Portland cement pastes has been studied via WAXS or wide-angle X-ray diffraction (WAXD) and USAXS techniques.

Materials and methods

Materials and preparation of cement pastes

Cement paste combinations were prepared using volcanic ash and ordinary Portland cement (OPC) type I. Ground volcanic ash was procured from Pozzolan Product Factory, Jeddah, Saudi Arabia. An in-house ball mill was used to grind the ash to a finer size, which was denoted as FA. The particle size distribution analysis was performed on volcanic ash and OPC by suspending them in isopropyl alcohol using a laser light scattering technique with a Micromeritics Saturn DigiSizer. The particle size analysis of volcanic ash and Portland cement is given in Table 1.

The chemical composition of OPC and volcanic ash was measured using X-ray florescence (XRF) spectroscopy, and the results are given in Table 2. The sum of silicon oxide (SiO_2), aluminum oxide (Al_2O_3) and ferric oxide (Fe_2O_3) components for the raw volcanic ash is 64.3%, indicating that the material is a Class C type of ash according to ASTM C 618 [26].

Methods

Cement paste combinations were prepared using dry mix of OPC and volcanic ash (see Table 3) and a 0.35 water-to-cement ratio. A water-to-cement ratio (w/c) of 0.35 was selected so that sufficient water is available to form hydration products and to facilitate incorporation of volcanic ash during the hydration process.

Ultra-small-angle X-ray scattering (USAXS), small-angle X-ray scattering (SAXS) and wide-angle X-ray scattering (WAXS)

USAXS and WAXS studies were conducted at USAXS beamline 9ID of the Advanced Photon Source (APS), Argonne National Laboratory, Lemont, IL [27, 28]. An X-ray energy of 18 keV was used to minimize multiple scattering and absorption in the sample. Using both the USAXS and SAXS detection modes, a small-angle scattering Q range from 0.0001 to 1.5 $Å^{-1}$ was used for this experiment; addition of WAXS extends this range to 6 $Å^{-1}$. Data were collected for 2.5 min per data set per specimen for 10 h. Prior to exposure to X-rays, it took about 2 min to prepare and mount the sample. USAXS data were reduced using the standard SAXS data analysis packages Indra and Nika that were developed at APS [27].

The absolute calibrated small-angle scattered intensity, $I(Q)$, was measured over several decades of the scattering vector magnitude, Q [29]:

$$Q = \frac{4\pi}{\lambda}\sin\left(\frac{\phi_s}{2}\right) \quad (1)$$

Table 1 Particle size analysis with two different particle sizes

Binder type	Nomenclature	Mean (μm)	Median (μm)	Mode (μm)	Diameter for selected percentiles by volume		
					D 90 (μm)	D 50 (μm)	D10 (μm)
Volcanic ash	IP	17.14	10.00	13.27	42.46	10.00	1.50
Volcanic ash	FA	6.40	3.25	2.97	15.79	3.25	0.97
Portland cement	OPC	12.73	7.94	6.65	30.10	7.94	2.12

Table 2 Chemical composition of OPC and volcanic ash

Binder type	Mass % as oxide									
	CaO	SiO_2	Al_2O_3	MgO	SO_3	TiO_2	K_2O	Fe_2O_3	Na_2O	P_2O_5
OPC	62.80	20.1	4.140	1.58	2.35	0.20	0.65	3.17	0.12	0.11
IP	9.29	47.0	14.80	7.95	0.14	2.41	1.40	12.5	3.54	0.61
FA	9.28	47.1	14.90	7.97	0.14	2.41	1.39	12.30	3.55	0.60

Table 3 Mix proportions and sample nomenclature

Nomination	Composition by dry weight (%)	
	OPC (%)	Volcanic ash (%)
OPC	100	0
IP-10	90	10
IP-30	70	30
IP-50	50	50
FA-10	90	10
FA-30	70	30
FA-50	50	50

OPC ordinary Portland cement; IP = OPC + volcanic ash (mean size: 17 μm); FA = OPC + volcanic ash (mean size: 6 μm)

where λ is the incident wavelength and ϕ_s is the scattering angle.

The scattering invariant was calculated by the Irena SAS package [20],

$$Q_{INV} = 2\pi^2\varphi(1-\varphi) * |\Delta\rho|^2 = \int_0^\infty Q^2 \frac{d\Sigma}{d\Omega}(Q)dQ \qquad (2)$$

where φ is the solid volume fraction, $\frac{d\Sigma}{d\Omega}(Q)$ is the differential scattering cross section and $\Delta\rho^2$ is the scattering contrast between pores and the solid. The solid volume fraction is the volume of the solid penetrated by the X-ray beam [30]. This can be used to indirectly measure of the amount of cementitious matrix, excluding the gel pores. The Irena tool program package [27] along with the model by Allen and Thomas [20] and Bumrongjaroen et al. [15] was used to analyze the scattering data and to obtain the specific surface area.

The specific surface area per unit specimen volume (S_T) can be determined by small-angle scattering as:

$$S_T = \frac{C_P}{2\pi|\Delta\rho|^2} \qquad (3)$$

where C_P is the Porod constant and $|\Delta\rho|^2$ is the scattering contrast between the voids and the solid phase. Porod constant (C_P) values can be obtained from the unconstrained intercepts of fits of Iq^4 versus q^4 [7]. The flat background scattering was subtracted out of both data and fit for convenience. In this study, unified fit tool in the Irena SAS package was used to determine the specific surface area.

Larger microstructure features can be related to the small-angle scattering results at the low Q range, whereas smaller features can be related to the results at the high Q range. At high Q values in the Porod regime, the intensity of the scattering becomes directly proportional to the total internal surface area of the specimen (see Fig. 1). In addition, a fractal microstructure model can be applied to the USAXS/SAXS data to determine the fractal exponent and fractal morphology of the C-S-H gels. A surface with roughness is known as surface fractal, whereas a fractal object with a network or cluster is known as the "mass or volume fractal" [31, 32].

It is worth mentioning here that, although X-ray scattering and neutron small-angle scattering are governed by the same formulas, they see the same

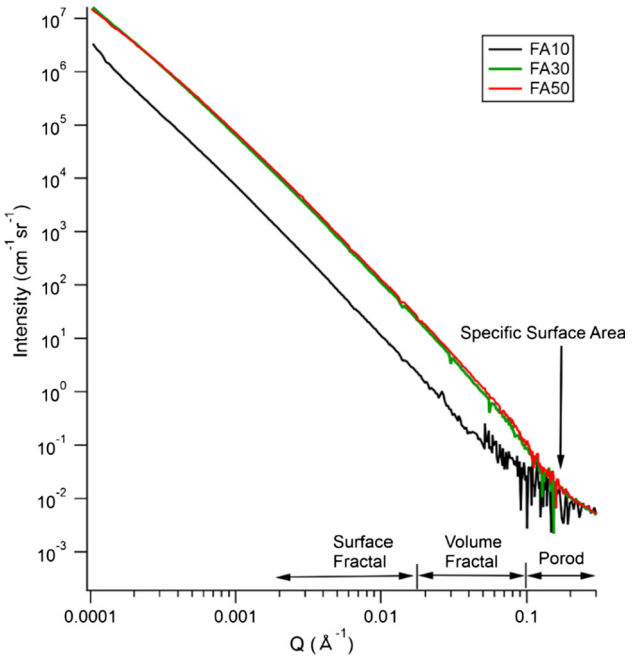

Figure 1 Experimental USAXS data collected on the cement pastes prepared with 6-μm-sized volcanic ash and Portland cement combination.

microstructures differently. Whereas X-ray scattering is dominated by heavier elements (denser electron cloud) and light elements scatter weakly, neutron scattering does not depend on element weight and in many cases light elements scatter more strongly that heavier ones. Thus, a combination of radiations can provide a more elaborate characterization of complex engineering materials.

Wide-angle X-ray scattering (WAXS)—also commonly referred to as powder diffraction or XRD—data from a 2D area detector were reduced for 2θ angle and intensity; these data were analyzed for phases using HighScore Plus software using ICDD database. The data were collected at a wavelength of 0.5904 Å and thus shift the peaks in 2θ compared to XRD obtained with Cu Kα radiation.

Results and discussion

Ultra-small-angle X-ray scattering (USAXS)

USAXS data were collected for 555 min with an 8–9-min time interval after initial mixing to track the immediate effect of volcanic ash with Portland cement during the early age of hydration (see Fig. 2a). The data were reduced to a standard data scattering cross section versus Q format with absolute intensity calibration and were desmeared to correct for slit smearing of the instrument geometry scattering cross section versus Q [27, 28]. For simplicity of analysis, the Q regions were divided into low (0.0001–0.001 Å^{-1}), medium (0.001–0.01 Å^{-1}) and high Q (0.01 to −1 Å^{-1}) regions. USAXS plots for OPC at low, medium and high Q values are shown in Fig. 2b–d. It is important to analyze the scattering data at a range of Q values to gain physical insight into the hydration process at a range of length scales, from smoother to coarser morphology. At lower Q values, larger microstructural features and surface fractal scattering result from the deposition of hydration product on the Portland cement and the resulting formation of a coarse surface [33]. At medium Q values, scattering is controlled by a volume fractal structure created by the random agglomeration of the C-S-H particles. High Q values are dominated by single-particle scattering that is affected by the form factor. Form factor, or shape factor, contains intraparticle information and relies on both the size and the shape of the scattering particle [34]. However, caution has to be exercised when analyzing polydisperse systems such as cement paste since the individual hydration products have different shapes, sizes and chemical compositions and therefore a single expression of form factor does not hold [35].

In the low Q regime after 9 min of hydration, a shift in the scattering was observed that can be attributed to the dissolution process. During hydration, the Portland cement, which contains C_3S, C_3A, C_2S and C_4AF, reacts with water while forming C-S-H along with other crystalline products such as portlandite. With the increase in the time of hydration, an increase in scattering intensity was observed and attributed to the formation of C-S-H gels. The development of C-S-H gel structure increases at high Q, while shrinking of unreacted cement clinker core diminishes at lower Q values [5].

The time dependencies of the changes in hydration at early age usually depend on the heat output from the hydration reactions that are affected by the concentration of volcanic ash in Portland cement. FA-10 sample consisting of 90% OPC and 10% volcanic ash of mean size 6 μm showed the least intensity at low, medium and high Q ranges (refer to Fig. 2). The IP specimens prepared with 17-μm volcanic ash showed an increase in intensity as the replacement of OPC with volcanic ash increased from 10 to 50%. IP-10

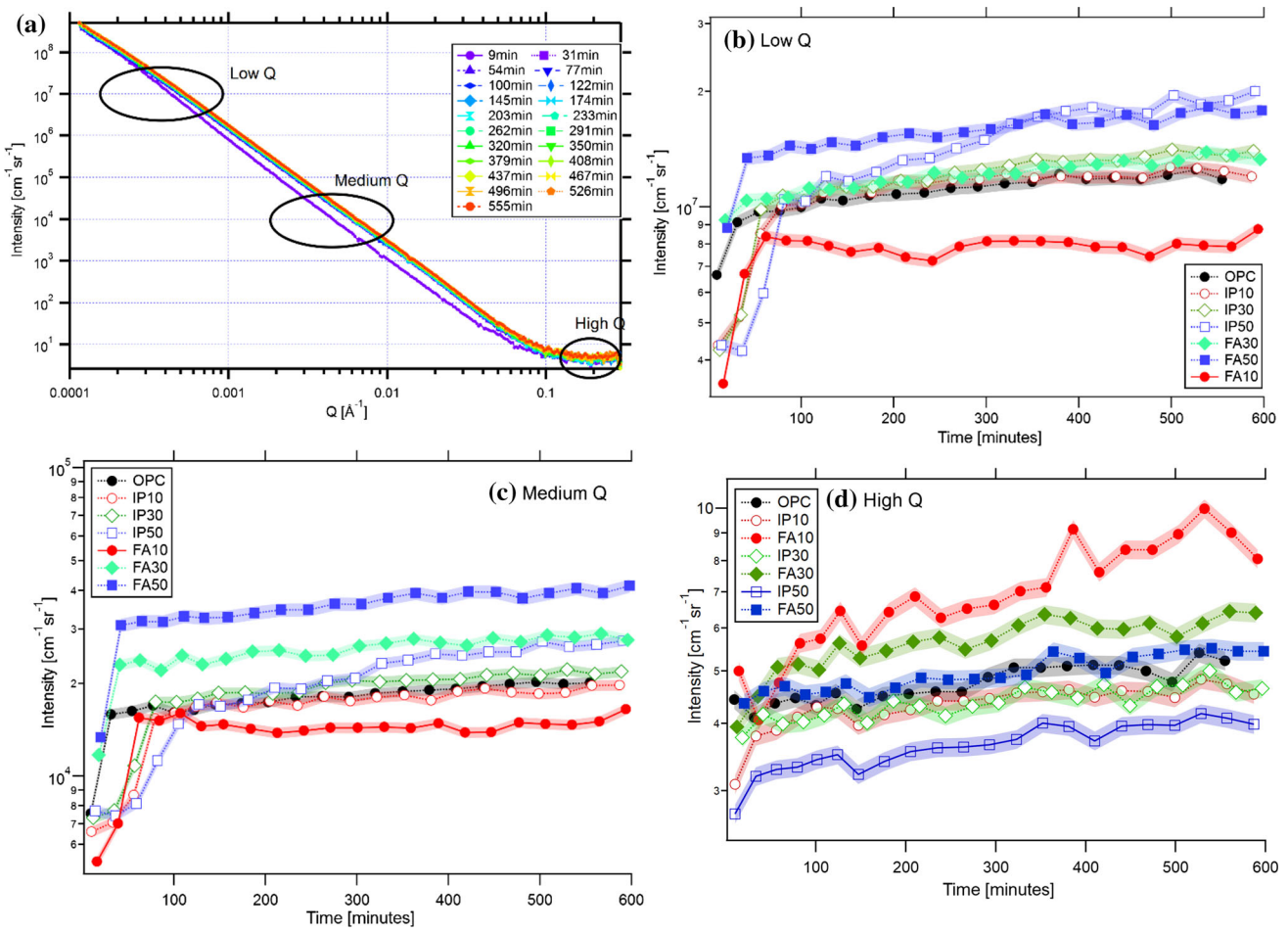

Figure 2 **a** USAXS intensity versus time plot of scattered intensity I (Q) versus wave vector Q (Å^{-1}) of ordinary Portland cement at 0.55 water-to-cement ratio, **b** at low $Q = 0.0005$ Å^{-1}, **c** at medium $Q = 0.005$ Å^{-1} and **d** high $Q = 0.02$ Å^{-1} (shading represents the error bars).

specimens had almost the same intensity as the OPC sample at low and medium Q, but slightly lower intensity in the high Q region. A detailed analysis of the data in low, medium and high Q regimes follows.

Low Q values correspond to larger microstructural features. At low Q values, the intensity is maximum for IP-50, followed by FA-50, IP-30, FA-30, IP-10, OPC and FA-10 (see Fig. 2b), because scattering intensity at lower Q correlates with larger microstructural features. These data suggest that samples with 50% volcanic ash had larger microstructural products and coarser morphology. FA-10 showed the least intensity at low Q, suggesting that the Portland cement clinker grains were consumed with the hydration time. Additionally, these data indicate that finer-sized volcanic ash is getting involved in the reaction forming smaller sizes and smoother surface hydration products.

At medium Q values, scattering is primarily dominated by volume or mass fractals, which correspond to random agglomeration of the C-S-H globules. In comparison with the low Q values, FA-50 had the highest intensity followed by FA-30, IP-50, IP-30, OPC, IP-10 and FA-10 in the medium Q region (see Fig. 2c). This indicates that FA-30 had a higher volume fractal than IP-50. Surface fractal deals with the roughness of only surfaces, whereas mass fractal deals with mass and surface systems alike [31, 32]. Volume fractal, also known as "mass fractal," is a structure accommodating branching and cross-linking to form a three-dimensional network [36]. For cement pastes prepared with 17-μm volcanic ash, an increase in volume fractal component with an increase in volcanic ash percentage from 10 to 50% was detected. However, when 6-μm-sized volcanic ash was used, FA-30 had the highest intensity,

suggesting that it had higher volume fractals than FA-50 and FA-10 samples. This suggests that an optimum limit exists around 30% substitution of OPC with volcanic ash that controls the fractal regimes which directly affect the hydration product formation even at the early age of curing.

In the high Q regime, smaller features are probed, and the response is mostly controlled by the formation of low-density C-S-H gel [37]. At high Q values, single-particle scattering dominates and relies on the form factor. In this study, the cement paste is a mixture of phases with different shapes/sizes, causing difficulty in distinguishing the single-particle scattering effect. In the high Q regime, FA-10 showed the highest intensity followed by FA-30 and FA-50. IP-50 had the least value in the high Q regime, signifying that as the concentration of 17-μm volcanic ash increased, the ash that was not involved in the hydration itself and instead contributed to the scattering (see Fig. 2c). Furthermore, because the low Q scattering is lower in some cases, which means that the ash is incorporated in the cementitious matrix, and thus, scattering is observed by the ash itself. Thus, it was concluded that reducing the particle size of volcanic ash from 17 to 6 μm facilitated its involvement in the hydration and thus resulted in lower scattering intensities among FA samples when compared to their IP counterparts.

In this situation, OPC has much finer particle size than volcanic ash (see Table 1), as the reaction progress when volcanic ash is blended with OPC leads to thicker reacted zone while resembling a volume fractal component. Additionally, at higher volcanic ash contents, greater contact between OPC and volcanic ash indicates a larger aluminosilicate source is available to react with water, forming rapid hydration products. These results are similar to the work performed by Allen and Livingston [8], which shows that addition of silica fume increased the surface area by forming a finer morphology indicating C-S-H formation. Compared to OPC, volcanic ash has high alumina and magnesium content, which contributes to the formation of heterogeneous phases consisting of C-S-H, C-A-S-H, and M-S-H [25]. Nonetheless, addition of volcanic ash can also generate significant C-S-H and other forms of C-S-H with varying Ca-to-Si ratios [38]. However, the significant increase in surface area due to 50% volcanic ash content may also be influenced by the net surface area of the volcanic ash itself that is not involved in the formation of C-S-H, C-A-S-H or other related hydration gels.

Surface area analysis

Specific surface area in m^2/g for first 600 min and after 58 days of hydration is shown in Fig. 3a, b, respectively. The USAXS power law slopes were measured from the scattering curves in the Q range from 0.0030 to 0.018 $Å^{-1}$. Surface area was obtained from the high Q values since the intensity of scattering is directly proportional to the total surface area. For the first 600 min of hydration, the surface area was the highest for FA-10 sample followed by FA-30 and FA-50. The IP samples had lower surface area compared to the FA counterparts for the first 600 min of hydration. At early age, the effect of particle size can be observed by lowering both particle size and concentration that led to higher surface area during the early age of hydration. The early-age surface area data suggest that increase in surface area from grinding the volcanic ash facilitates

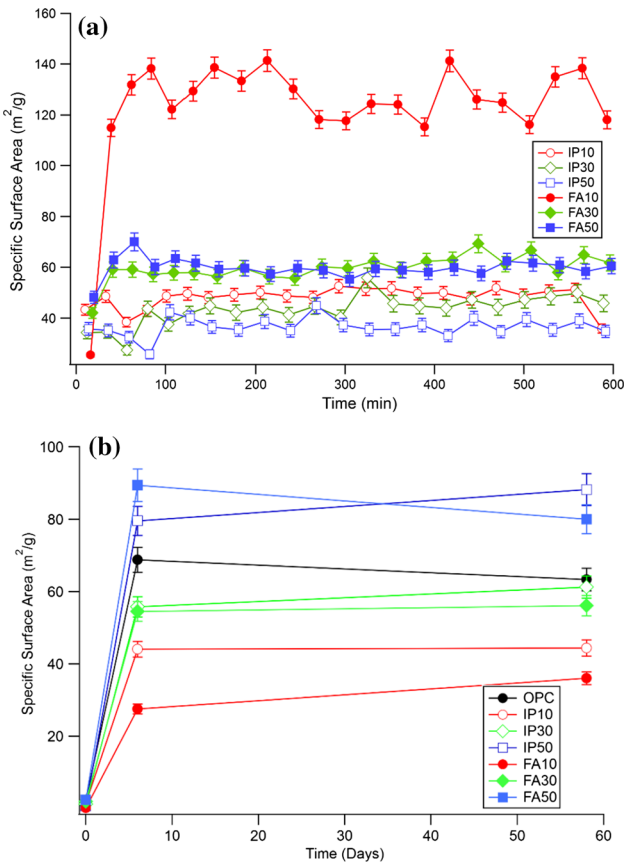

Figure 3 **a** Specific surface area at early age during the first 600 min of hydration, **b** surface area 6 and 58 days of curing.

involvement of the ash during the gelation process. Increases in surface area are attributed to initiation of the gelation process as the clinker particles are dissolved and subsequently agglomerate [39]. At early age, the high surface area is attributed to an increased capacity for the volcanic ash to react with the free water, forming chemically bound water inside the calcium-silicate-hydrate gels. Furthermore, this work supports past quasielastic neutron scattering (QENS) results that demonstrated the presence of free water for mixes where higher concentrations and larger-sized volcanic ash partially replaced Portland cement [9].

Furthermore, first-day reactions have further implications on the amount of remaining available unreacted volcanic ash and free water, as can be seen on 6- and 58-day data (Fig. 3b). For example, FA-50 had a higher specific surface area than IP-50 up until day 6 because finer volcanic ash particles had a higher surface area interface since free water is available for the reaction. Since these samples were prepared with a water-to-cement (w/c) ratio of 0.35 to ensure that sufficient free water is available even after the cement paste is hydrated. After 58 days of hydration, the specimens with higher volcanic ash concentration produced higher surface area which is in contrast as compared to the early-age data (refer to Fig. 3a). For IP-50, there was more free water remaining by day 58 such that the earlier hydration products continued to react until day 58 using the remaining free water. Therefore, IP-50 had a higher specific surface area calculation than FA-50 at day 58. This suggests that addition of higher concentration of volcanic ash facilitates secondary pozzolanic reaction due to the availability of free water, which is available in high concentration of volcanic ash-OPC combinations. Although an analysis of the specific surface area can show the timing and extent of hydration reactions, it does not provide any insight as to which reaction and which hydration products are involved. Nevertheless, these results can be complemented by a phase analysis of in situ WAXS data, which provides insight about which phases are present at each specific time.

In situ wide-angle X-ray scattering (WAXS)

WAXS data were collected for hydrating OPC from 7 to 120 min as shown in Fig. 4. As expected of standard OPC cement paste, consumption of C_3S phase and crystallization of calcium hydroxide was observed in this control sample. As the hydration proceeded, a decrease in the C_3S peak along with corresponding increases in Portlandite and C-S-H in the form of rosenhahnite [$Ca_3Si_3O_8$ $(OH)_2$] was detected. Rosenhahnite is attributed to the reflection of the C-S-H family [40, 41]. This phase is responsible for the crystal growth of the C-S-H particulates, thus facilitating the seeding effect in the C-S-H gels [42].

WAXS analysis for IP-30 and FA-30 at 6, 29, 52, 74, 97 and 120 min is shown in Fig. 5a, b, respectively. Addition of IP and FA volcanic ash led to the formation of gismondine and heulandite-Ca, respectively, which is related to the formation of calcium-aluminum-silicate-hydrate (C-A-S-H) gels. Furthermore, C-S-H phases in the form of rosenhahnite and oyelite were observed among IP-30 and FA-30, respectively.

Presence of gismondine indicated traces of intermediate C-A-S-H gel phase due to the presence of alumina content in the volcanic ash. Moreover, gismondine has been attributed to encapsulated water ions and thus at a later stage could facilitate additional hydration [43], as seen by USAXS analysis. Occurrence of heulandite-Ca was detected among FA-30 samples and was observed due to the increase in Al and Ca content from the volcanic ash. It has also been observed that these zeolitic-type phases are expected to precipitate within these binders and contribute to additional strength of the cementitious matrix [44, 45].

It is important to note that the regular volcanic ash was ground in a high-speed ball mill to a finer size and during grinding a temperature increase of up to 100 °C may have contributed to the destruction of the heulandite crystals. Zeolites which are neocrystallized due to heating are difficult be detect via XRD. A previous study showed that zeolites that are altered and destructed due to heat are responsible for precipitation reactions that increase the pozzolanic activity of the cementitious binders [45].

C-S-H phases of rosenhahnite [$Ca_3Si_3O_8(OH)_2$] and oyelite ($Ca_{10}B_2Si_8O_{29}{\cdot}12.5H_2O$) were detected among IP-30 and FA-30 specimens, respectively. Rosenhahnite is related to the C-S-H family, whereas oyelite belongs to the tobermorite group [46]. Oyelite is a 1.4-nm tobermorite structure with the bridging tetrahedral either missing or replaced by borate groups. Using nuclear magnetic resonance (NMR), oyelite has been assigned to dimers (Q^1) or to Q^2 sites affected by

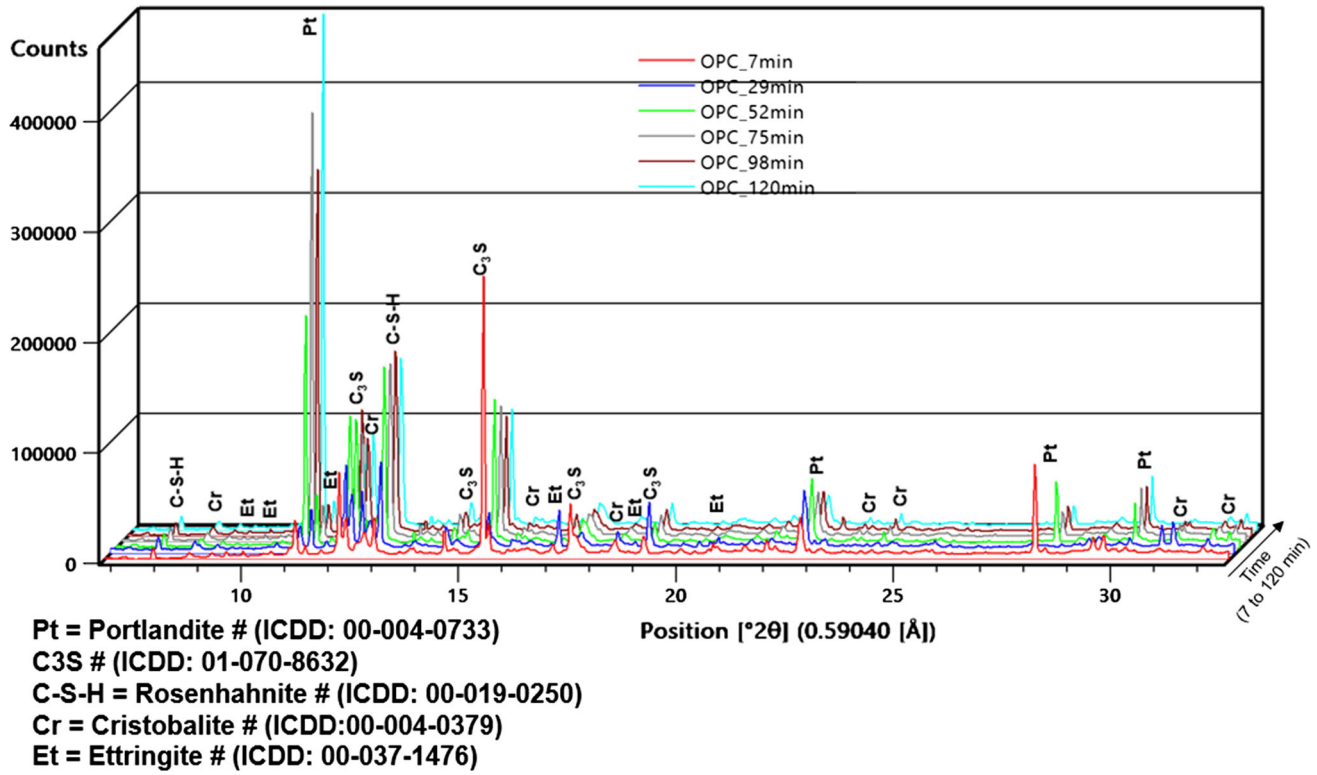

Figure 4 Wide-angle X-ray scattering for hydrating ordinary Portland cement (OPC) paste.

BO_4 in oyelite [47, 48]. These results illustrate that grinding the volcanic ash from 17 to 6 μm resulted in changes in the C-S-H structure. This suggests that changes in the base volcanic ash structure led to different crystallized forms of C-S-H, although these changes may also be attributed to a temperature increase undergone during grinding.

It is interesting to note that in FA samples, a zeolitic phase of scolecite was detected at 29 min of hydration, but this strong peak disappears after 52 min (see Fig. 5b). This zeolitic phase was not observed among IP samples as shown in Fig. 5a. Scolecite phase [$CaAl_2Si_3O_{10}{\cdot}3(H_2O)$] is commonly observed in basaltic rock 226–282 m below the Earth's surface [49]. This phase is attributed to the 6-μm volcanic ash that did not begin to react until between 29 and 52 min of hydration. Furthermore, these zeolitic phases such as scolecite were not observed among IP-30 during the first 120 min of hydration. This suggests that grinding IP (17 μm) to FA (6 μm) helps in early-age reactions of the zeolitic phases by involving the volcanic ash in the hydration reaction.

WAXS analysis for all samples after 58 days of hydration is given in Table 4. The IP-10 sample showed the presence of α-C-S-H and rosenhahnite, while IP-50 had only α-C-S-H and more C-A-S-H gel-dominated phases (heulandite-Ca and chabazite-Ca). In contrast, all the FA combinations showed different forms of C-S-H phase, whereas FA-10 did not show any major C-A-S-H phases as compared to FA-30, which had traces of heulandite-CA, and FA-50, which had traces of yugawaralite and gismondine phases. Furthermore, more than 30% substitution of volcanic ash facilitated domination of C-A-S-H gel phases for both IP and FA samples. This also suggests that grinding the volcanic ash facilitated formation of C-S-H phases than of C-A-S-H gel, which could be correlated with transformation in the crystal structure due to heat produced while grinding. Studies have shown that subjecting natural pozzolans to low thermal heating facilitates pozzolanic reactions that result in additional C-S-H that contributed to higher strength in comparison with the non-heated pozzolans in Portland cement-based systems [45].

After 58 days, hydration of cement paste was affected by atmospheric carbonation by forming different polymorphs of carbonates. IP-50 showed the presence of vaterite, whereas the other samples had the presence of calcite and aragonite. The absence of calcite peaks and occurrence of vaterite in IP-50

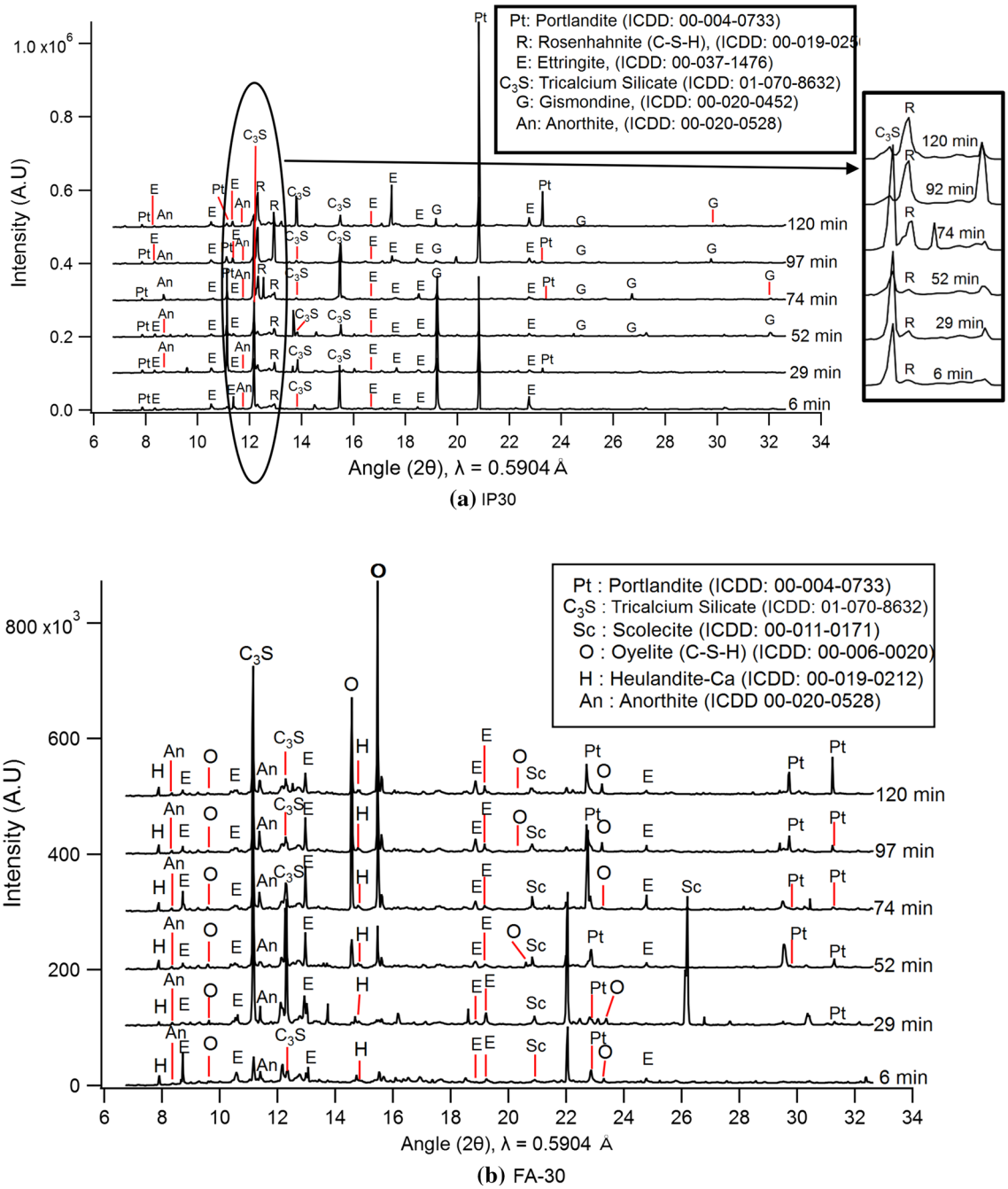

Figure 5 WAXS data analysis for 30% replacement of Portland cement with volcanic ash of mean size of **a** 17 μm (IP-30) and **b** 6 μm (FA-30).

suggests that carbonates are forming inside the calcium-aluminate-hydrate phases and inside the C-S-H gels [48].

IP-50 showed traces of dolomites, while brucite, which is a crystalline form of magnesium hydroxide, was observed FA-10, FA-30 and IP-10 samples. It is known that C-S-H can incorporate Mg ions in the form of brucite, which results in the reduction of Portlandite and hinders the precipitation reaction that leads to the formation of C-S-H and Portlandite phases [50]. Additional alumina and silica from the volcanic ash may have reacted with the available Mg to form magnesium-silicate-hydrate (M-S-H) ($3MgO{\cdot}2SiO_2{\cdot}2H_2O$), which is amorphous in nature. Subsequently, the crystallization of the $Mg(OH)_2$ by-product would lead to the formation of brucite. The

Table 4 Phase analysis using WAXS data on samples after 58 days

Phase	Formula	Specimen combinations						
		OPC	FA10	FA30	FA50	IP10	IP30	IP50
Portlandite	$Ca(OH)_2$	×		×	×	×	×	×
Calcio-olivine	Ca_2SiO_4			×				×
Clino-tobermorite	$Ca_5Si_6O_{17}·5H_2O$	×						
Tobermorite	$Ca_5Si_6O_{16}(OH)_2$	×						
α-C-S-H	$Ca_2(HSiO_4)(OH)$		×			×		×
Hillebrandite	$Ca_2(SiO_3)(OH)_2$		×					
Oyelite	$Ca_{10}B_2Si_8O_{29}·12.5H_2O$			×	×		×	
Rosenhahnite	$Ca_3Si_3O_8(OH)_2$			×	×	×	×	
Okenite	$[Ca_8(Si_6O_{16})(Si_6O_{15})_2\ (H_2O)_6]^{4-}[Ca_2(H_2O)_9·3H_2O]^{4+}$			×				
Scolecite	$CaAl_2Si_3O_{10}·3(H_2O)$			×			×	×
Heulandite-Ca	$Ca_{1.07}Al_{2.14}Si_{6.86}O_{18}·6.17H_2O$			×			×	×
Yugawaralite	$CaO·Al_2O_3·6Si_6O_2·4(H_2O)$				×			
Gismondine	$Ca_2Al_4Si_4O_{16}·9(H_2O)$				×			
Chabazite-Ca	$(Ca_{0.5},Na,K)4[Al_4Si_8O_{24}]·12H_2O$					×	×	×
Aragonite	$CaCO_3$ (orthorhombic)	×	×					
Vaterite	$CaCO_3$ (hexagonal)							×
Calcite	$CaCO_3$ (trigonal)					×	×	
Dolomite	$CaMg(CO_3)_2$		×			×		×
Thenardite	Na_2SO_4	×	×	×	×		×	
Cristobalite	SiO_2	×						
Quartz	SiO2				×			
Brucite	$Mg(OH)_2$		×	×		×		
Periclase	MgO			×	×	×	×	
Gibbsite	Γ-Al $(OH)_3$	×						
Diaspore	AlO(OH)					×		×

following equation shows the formation of M-S-H gels [51].

$$4Mg^{2+} + 2SO_4^{2-} + 2[CaO \cdot SiO_2aq] + 8H_2O \rightarrow 3MgO \cdot 2SiO_2 \cdot 2H_2O + 2[CaSO_4 \cdot 2H_2O] + Mg(OH)_2 \quad (4)$$

Previous study on a nanometer scale revealed that C-S-H gels form polydisperse multilayer disks, while M-S-H globules are a combination of small and large polydispersed spheres in the range of 30–50 nm diameter [22]. The differences in the basic building blocks of C-S-H and M-S-H phases reflect the distinction in the morphological phases at larger length scales. The differences in shape, length scale and density between the M-S-H and C-S-H gels lead to compatibility problems. Moreover, M-S-H gels are weaker in strength than C-S-H gels due to the presence of increased porosity in the M-S-H gels. Recent strength studies have shown that greater than 30% addition of volcanic ash to OPC contributed to lower compressive and flexural strengths [23, 25].

Overall Discussion

Advanced synchrotron techniques were used to observe the early-age hydration behavior when two different-sized natural pozzolanic volcanic ashes were each used as a partial substitute to Portland cement. Combining USAXS, SAXS and WAXS data with SAS and XRD-like data analysis techniques helped in understanding the morphology and growth of the cementitious products ranging from angstrom to micron size that could have affected the surface area during the hydration process. USAXS–SAXS–WAXS provides vital insights into the mix design when additives are used as supplementary cementitious materials along with OPC to prepare engineered concretes.

USAXS data analysis at low Q regime between 0.0001 and 0.001 $Å^{-1}$ showed that concentration and particle size of volcanic ash played a major role in controlling the microstructural growth resulting in larger features for IP-50 which corresponds to 50% substitution of OPC with finely ground volcanic ash (17 μm). The medium Q analysis in the range of 0.001 Å–0.01 $Å^{-1}$ provided critical insight into the fractal structure of the resulting hydration product that could affect the surface roughness depending on the amount and particle size of the volcanic ash substitution. High Q analysis (0.01–1 $Å^{-1}$) probes the smaller features, and this analysis concluded that remnant unreacted IP volcanic ash (17 μm) itself contributed to scattering. Furthermore, high Q analysis showed that finer the size of volcanic ash higher was the surface area during early age (up to 10 h) while at the later age (58 days), the volcanic ash itself can contribute to partial hydration that resulted in increased surface for 50% substituted samples.

WAXS analysis revealed phases related to three major building blocks, C-S-H, C-A-S-H and M-S-H. Addition of regular-sized volcanic ash (17 μm) contributed to C-A-S-H- and M-S-H-related phases due to increasing Al, Si and Mg content from the volcanic ash. However, specimens prepared with fine ground ash (6 μm) were dominated by C-S-H-related phases. Since C-S-H has a disk-like polydisperse shape and M-S-H possesses a spherical morphology, the disparity among these shapes may have led to increases in surface area among samples with high volcanic ash substitution (IP-50 and FA-50).

These results show that greater than 30% substitution of volcanic ash leads to unreacted volcanic ash and coarser morphology, which could influence the mechanical properties of the resulting hydration products. The study also provides insights into predissolution period, which could affect the resulting gel formation leading to multi-component morphology. This work indicates that supplementary cementitious materials such as volcanic ash form a complex morphology and affect the early-age evolution of gels. Therefore, additional studies are required to characterize the pure synthetic C-S-H, C-A-S-H, M-S-H and combinations of these gels using USAXS and WAXS techniques.

However, caution has to be observed when analyzing hydration of cements with X-rays because they can expedite the setting time during the initial course of hydration. This trend is difficult to observe with neutron scattering, which detected a steady decrease in intensity, while the X-ray scattering first detected an increase followed by a decrease in intensity. The decrease in intensity suggests that the clinker grains are converted to a much finer scale, developing a nanoscale gel-like morphology related to C-S-H-type hydration products of approximately 5 nm in size [52]. The gelation process is accompanied by nucleation and growth, followed by reorganization, which continues in subtle ways even after the cement paste is completely hydrated. Furthermore, the variation in the scattering intensity is attributed to the gel/pore interface that is developed during early age of hydration [34].

Conclusions

Cement paste is a highly used, but energy-intensive, material for which volcanic ash, an abundant and natural resource, is a sustainable alternative. Thus, this study explored mixes of ordinary Portland cement substituted by different amounts (10, 30 and 50%) of pozzolanic volcanic ash. Powerful and non-invasive techniques (USAXS and WAXS) were used in situ to better understand the nano- and microstructures during early-age hydration.

The current work provides vital insight into the colloidal aspects of early-age kinetics when volcanic ash, a natural additive, is used as a partial substitute to Portland cement. The current study is the first study to use USAXS and WAXS to study mixes of volcanic ash and OPC at different concentrations. The suspended colloidal particles formed at the early age of the hydration reaction of cement pastes blended with volcanic ash were examined by following the scattering intensity and surface area via USAXS and by identifying phases using WAXS during the dissolution and gel initiation stage.

The main findings are as follows:

- The intensity analysis at different Q values showed that 10% FA ash (mean value of 6 μm) was more involved in the hydration process, whereas 50% ash with 17 μm (IP-50) to the mix led to coarser microstructural products.
- The specific surface area results suggested that grinding the volcanic ash to 6 μm facilitated involvement of volcanic ash with OPC resulting in increased surface area which is partially

attributed to the formation of C-S-H, C-A-S-H and M-S-H.

- WAXS studies showed that addition of volcanic ash facilitated the formation of C-S-H-related phases whereas inclusion of coarser volcanic ash was dominated by C-A-S-H and unreacted MgO phases suggesting un-involvement of volcanic ash in the hydration process.
- Increase in surface area per unit volume was observed as the volcanic ash content increased in the mix, suggesting a multi-component hydration product formation. The data showed that inclusion of volcanic ash greater than 30% led to a coarser morphology by affecting the initial pre-dissolution period, and it led to abrupt dissolution that could retard gelation of hydration products.
- The concentration of volcanic ash impacts the morphology and surface area, and it suggests an optimum limit for substitution of Portland cement with volcanic ash lies between 10 and 30% substitution.

Based on the above finding, this work contributes to a gap in research on natural cementitious materials, in spite of its first use by the ancient Romans almost 2000 years ago [3]. It provides a basis for future studies that tailor natural pozzolans-like volcanic ash as an effective additive for developing durable cements for specific applications. Additionally, it provides a basis for studying the influence of volcanic ash on individual hydration products (C-S-H, C-A-S-H and M-S-H) which could significantly affect the chemo-mechanical properties of engineered cementitious binders.

Acknowledgements

Use of the Advanced Photon Source (APS), an Office of Science User Facility operated for the U.S. Department of Energy (DOE) Office of Science by Argonne National Laboratory, was supported by the U.S. DOE under Contract No. DE-AC02-06CH11357. This work utilized facilities supported in part by the National Science Foundation under Agreement No. DMR-1508249. We thank the "Kuwait Foundation for the Advancement of Sciences" and "Kuwait-MIT Center for Natural Resources and the Environment" for their support during this work. We also acknowledge fruitful discussion with Dr. Andrew Allen from the Materials Structure and Data Group in the Materials Measurement Science Division at NIST. We thank Dr. Charlie Settens from CMSE, MIT for his help in WAXS data analysis. The authors are also thankful to the Pozzolan Product Factory located in Jeddah, Saudi Arabia, for providing the volcanic ash for this experimental study.

References

[1] Ottewill RH, Sing KSW, Bensted J (1983) Chemistry of colloidal silicates and cements and discussion. Philos Trans R Soc Lond Ser A Math Phys Sci 310(1511):67–78. doi:10.1098/rsta.1983.0066

[2] Chiang W-S, Fratini E, Ridi F, Lim S-H, Yeh Y-Q, Baglioni P, Choi S-M, Jeng US, Chen S-H (2013) Microstructural changes of globules in calcium–silicate–hydrate gels with and without additives determined by small-angle neutron and X-ray scattering. J Colloid Interface Sci 398:67–73. doi:10.1016/j.jcis.2013.01.065

[3] Ridi F, Fratini E, Baglioni P (2011) Cement: a two thousand year old nano-colloid. J Colloid Interface Sci 357(2):255–264. doi:10.1016/j.jcis.2011.02.026

[4] Nicoleau L, Gadt T, Chitu L, Maier G, Paris O (2013) Oriented aggregation of calcium silicate hydrate platelets by the use of comb-like copolymers. Soft Matter 9(19):4864–4874. doi:10.1039/C3SM00022B

[5] Allen AJ, Oberthur RC, Pearson D, Schofield P, Wilding CR (1987) Development of the fine porosity and gel structure of hydrating cement systems. Philos Mag Part B 56(3):263–288. doi:10.1080/13642818708221317

[6] Allen AJ, Thomas JJ, Jennings HM (2007) Composition and density of nanoscale calcium-silicate-hydrate in cement. Nat Mater 6(4):311–316. http://www.nature.com/nmat/journal/v6/n4/suppinfo/nmat1871_S1.html

[7] Thomas JJ, Jennings HM, Allen AJ (1998) The surface area of cement paste as measured by neutron scattering: evidence for two C-S-H morphologies. Cem Concr Res 28(6):897–905. doi:10.1016/S0008-8846(98)00049-0

[8] Allen AJ, Livingston RA (1998) Relationship between differences in silica fume additives and fine-scale microstructural evolution in cement based materials. Adv Cem Based Mater 8(3–4):118–131. doi:10.1016/S1065-7355(98)00015-7

[9] Kupwade-Patil K, Tyagi M, Brown CM, Büyüköztürk O (2016) Water dynamics in cement paste at early age prepared with pozzolanic volcanic ash and Ordinary Portland Cement using quasielastic neutron scattering. Cem Concr Res 86:55–62. doi:10.1016/j.cemconres.2016.04.011

[10] Barker AP (1989) An electron optical examination of zoning in blastfurnace slag hydrates: part I. Slag cement pastes at early ages. Adv Cem Res 2(8):171–179. doi:10.1680/adcr.1989.2.8.171

[11] Snellings R, Mertens G, Cizer Ö, Elsen J (2010) Early age hydration and pozzolanic reaction in natural zeolite blended cements: reaction kinetics and products by in situ synchrotron X-ray powder diffraction. Cem Concr Res 40(12):1704–1713. doi:10.1016/j.cemconres.2010.08.012

[12] Chotard TJ, Boncoeur-Martel MP, Smith A, Dupuy JP, Gault C (2003) Application of X-ray computed tomography to characterise the early hydration of calcium aluminate cement. Cem Concr Compos 25(1):145–152. doi:10.1016/S0958-9465(01)00063-4

[13] Juenger MCG, Winnefeld F, Provis JL, Ideker JH (2011) Advances in alternative cementitious binders. Cem Concr Res 41(12):1232–1243. doi:10.1016/j.cemconres.2010.11.012

[14] Gastaldi D, Canonico F, Capelli L, Boccaleri E, Milanesio M, Palin L, Croce G, Marone F, Mader K, Stampanoni M (2012) In situ tomographic investigation on the early hydration behaviors of cementing systems. Constr Build Mater 29:284–290. doi:10.1016/j.conbuildmat.2011.10.016

[15] Bumrongjaroen W, Livingston RA, Neumann DA, Allen AJ (2009) Characterization of fly ash reactivity in hydrating cement by neutron scattering. J Mater Res 24(07):2435–2448. doi:10.1557/jmr.2009.0267

[16] Allen AJ, Windsor CG, Rainey V, Pearson D, Double DD, Alford NM (1982) A small-angle neutron scattering study of cement porosities. J Phys D Appl Phys 15(9):1817–1834

[17] Livingston RA, Neumann DA, Allen A, RUSH JJ (1994) Application of neutron scattering methods to cementitious materials. In: MRS online proceedings library 376. doi:10.1557/PROC-376-459

[18] Chiang W-S, Fratini E, Baglioni P, Liu D, Chen S-H (2012) Microstructure determination of calcium-silicate-hydrate globules by small-angle neutron scattering. J Phys Chem C 116(8):5055–5061. doi:10.1021/jp300745g

[19] Phair JW, Schulz JC, Bertram WK, Aldridge LP (2003) Investigation of the microstructure of alkali-activated cements by neutron scattering. Cem Concr Res 33(11):1811–1824. doi:10.1016/S0008-8846(03)00199-6

[20] Allen AJ, Thomas JJ (2007) Analysis of C-S-H gel and cement paste by small-angle neutron scattering. Cem Concr Res 37(3):319–324. doi:10.1016/j.cemconres.2006.09.002

[21] Thomas JJ, Jennings HM (2006) A colloidal interpretation of chemical aging of the C-S-H gel and its effects on the properties of cement paste. Cem Concr Res 36(1):30–38. doi:10.1016/j.cemconres.2004.10.022

[22] Chiang W-S, Ferraro G, Fratini E, Ridi F, Yeh Y-Q, Jeng U, Chen S-H, Baglioni P (2014) Multiscale structure of calcium-and magnesium-silicate-hydrate gels. J Mater Chem A 2(32):12991–12998

[23] Al-Bahar S, Chakkamalayath J, Joseph A, Abdulsalam M, Al-Otaibi S, Al-Aibani A (2017) Effect of volcanic ash incorporation on the mechanical properties and surface morphology of hydrated cement paste. J Mater Civ Eng. doi:10.1061/(ASCE)MT.1943-5533.0001886

[24] Husain A, Kupwade-Patil K, Al-Aibani AF, Abdulsalam MF (2017) In situ electrochemical impedance characterization of cement paste with volcanic ash to examine early stage of hydration. Constr Build Mater 133:107–117. doi:10.1016/j.conbuildmat.2016.12.054

[25] Kupwade-Patil K, Al-Aibani AF, Abdulsalam MF, Mao C, Bumajdad A, Palkovic SD, Büyüköztürk O (2016) Microstructure of cement paste with natural pozzolanic volcanic ash and Portland cement at different stages of curing. Constr Build Mater 113:423–441. doi:10.1016/j.conbuildmat.2016.03.084

[26] ASTM (2004) Standard specification for coal fly ash and raw or calcined natural pozzolan for use in concrete. ASTM C 618-12a. ASTM International, West Conshohocken

[27] Ilavsky J, Jemian PR (2009) Irena: tool suite for modeling and analysis of small-angle scattering. J Appl Crystallogr 42(2):347–353

[28] Ilavsky J, Jemian PR, Allen AJ, Zhang F, Levine LE, Long GG (2009) Ultra-small-angle X-ray scattering at the advanced photon source. J Appl Crystallogr 42(3):469–479. doi:10.1107/s0021889809008802

[29] Glatter O, Kratky O (1982) Small angle X-ray scattering. Academic Press, New York

[30] Trapote-Barreira A, Porcar L, Cama J, Soler JM, Allen AJ (2015) Structural changes in C-S-H gel during dissolution: small-angle neutron scattering and Si-NMR characterization. Cem Concr Res 72:76–89. doi:10.1016/j.cemconres.2015.02.009

[31] Russ JC (2013) Fractal surfaces. Springer, Berlin

[32] Avnir D (1989) The fractal approach to heterogeneous chemistry: surfaces, colloids, polymers. Wiley, New York

[33] Thomas JJ, Allen AJ, Jennings HM (2008) Structural changes to the calcium–silicate–hydrate gel phase of hydrated cement with age, drying, and resaturation. J Am Ceram Soc 91(10):3362–3369. doi:10.1111/j.1551-2916.2008.02636.x

[34] Aligizaki K (2005) Pore structure of cement-based materials: testing interpretation and requirements. Taylor & Francis, Abingdon

[35] Feigin LA, Svergun DI (2013) structure analysis by small-angle X-ray and neutron scattering. Springer, Berlin

[36] Hammouda B (2009) Probing nanoscale structures-the sans toolbox. National Institute of Standards and Technology Center for Neutron Research, Gaithersburg, MD, pp 20899–26102

[37] Thomas JJ, Chen JJ, Allen AJ, Jennings HM (2004) Effects of decalcification on the microstructure and surface area of cement and tricalcium silicate pastes. Cem Concr Res 34(12):2297–2307. doi:10.1016/j.cemconres.2004.04.007

[38] Massazza F (2002) Properties and applications of natural pozzolanas. In: Structure and performance of cements, pp 326–352

[39] Bullard JW, Jennings HM, Livingston RA, Nonat A, Scherer GW, Schweitzer JS, Scrivener KL, Thomas JJ (2011) Mechanisms of cement hydration. Cem Concr Res 41(12):1208–1223. doi:10.1016/j.cemconres.2010.09.011

[40] Richardson GI (2000) The nature of the hydration products in hardened cement pastes. Cem Concr Compos 22:97–113

[41] Richardson IG (1999) The nature of C-S-H in hardened cements. Cem Concr Res 29(8):1131–1147. doi:10.1016/S0008-8846(99)00168-4

[42] Gastaldi D, Paul G, Marchese L, Irico S, Boccaleri E, Mutke S, Buzzi L, Canonico F (2016) Hydration products in sulfoaluminate cements: evaluation of amorphous phases by XRD/solid-state NMR. Cem Concr Res 90:162–173. doi:10.1016/j.cemconres.2016.05.014

[43] De Silva PS, Glasser FP (1993) Phase relations in the system $CaO{\cdot}Al_2O_3{\cdot}SiO_2{\cdot}H_2O$ relevant to metakaolin—calcium hydroxide hydration. Cem Concr Res 23(3):627–639. doi:10.1016/0008-8846(93)90014-Z

[44] Myers RJ, Bernal SA, Provis JL (2017) Phase diagrams for alkali-activated slag binders. Cem Concr Res 95:30–38. doi:10.1016/j.cemconres.2017.02.006

[45] Habert G, Choupay N, Montel JM, Guillaume D, Escadeillas G (2008) Effects of the secondary minerals of the natural pozzolans on their pozzolanic activity. Cem Concr Res 38(7):963–975. doi:10.1016/j.cemconres.2008.02.005

[46] Richardson IG (2008) The calcium silicate hydrates. Cem Concr Res 38(2):137–158. doi:10.1016/j.cemconres.2007.11.005

[47] Maeshima T, Noma H, Sakiyama M, Mitsuda T (2003) Natural 1.1 and 1.4 nm tobermorites from Fuka, Okayama, Japan: chemical analysis, cell dimensions, 29Si NMR and thermal behavior. Cem Concr Res 33(10):1515–1523. doi:10.1016/S0008-8846(03)00099-1

[48] Taylor HFW (1997) Cement chemistry, 2nd edn. Thomas Telford, London

[49] Marks N, Schiffman P, Zierenberg RA, Franzson H, Fridleifsson GÓ (2010) Hydrothermal alteration in the Reykjanes geothermal system: insights from Iceland deep drilling program well RN-17. J Volcanol Geotherm Res 189(1–2):172–190. doi:10.1016/j.jvolgeores.2009.10.018

[50] Fernandez L, Alonso C, Andrade C, Hidalgo A (2008) The interaction of magnesium in hydration of C3S and CSH formation using 29Si MAS-NMR. J Mater Sci 43(17):5772–5783. doi:10.1007/s10853-008-2889-2

[51] Alexander M, Bertron A, De Belie N (2012) Performance of cement-based materials in aggressive aqueous environments: state-of-the-art report, RILEM TC 211 - PAE. Springer, Berlin

[52] Masoero E, Del Gado E, Pellenq RJM, Ulm FJ, Yip S (2012) Nanostructure and nanomechanics of cement: polydisperse colloidal packing. Phys Rev Lett 109(15):155503